CO12-1

Effective Measures on Safety, Security, Hygiene and Disaster Prevention in Laboratories

T. Iimoto[1], Y. Cai[1], Q. Jin[1], C. Guh[1], X. Wang[1], T. Kose[1], Y. Taniguchi[1], K. Takamiya[2]

[1]*The University of Tokyo*
[2]*Integrated Radiation and Nuclear Science, Kyoto University*

INTRODUCTION: Important aspects of the study can be found in the following keywords, such as safety, security, hygiene and disaster prevention. Nuclear research reactors are one of the representative facilities together with these keywords under their operation. It is effective to investigate the latest status on practical measures on these keywords in various facilities including nuclear research reactors, to compare each other among facilities, and to discuss more optimized ones for our positive safety management. Through this process, it is also essential to investigate the latest international and/or national regulations and the movement of revision of them. In addition, the development of human resources and public literacy on nuclear science and technology is also within the scope of the research. The total discussion contents and their fruits are directly useful for all relating laboratories.

RESEARCH APPROACH: General research approach is as follows.
- Measures of safety management during operation or standstill status of the real facilities would be investigated. This information would be used for our research discussion on positive and more optimized safety management. - It would not be a single year research, but maybe two to three years of research for one theme. - Information source of facilities would not be only KUR, KUCA or the other facilities in Kyoto University, but also the Kindai university research nuclear reactor or the facility of National Institute of Fusion Science, etc. This research is active joint-research with these related facilities and positive researchers on safety management. - One of the distinctive features of this research is to involve office staff as cooperators as well as re-searchers and technical staff. In The University of Tokyo, most of the members in Division for Environment, Health and Safety are office staff who know the real situation of safety management in laboratories very well.

Concrete discussion targets in FY of 2024 were determined as (1) ‘developing a set of educational videos for radiation protection in English for International Nuclear Science and Technology Academy (INSTA)’ and (2) ‘Investigation of the latest trends in Japan and overseas regarding the optimized management of X-rays’. These were the representative hottest topics in the field of radiation protection and safety.

RESULTS: <CONCEPT AND CONTENTS OF RP-EDU-VIDEO> To support the INSTA activity, the research team developed three English videos entitled as ‘General Risk Management’, ‘Medical Risk Management’, and ‘Chemical Risk Management’, which were planned to be applied in INSTA Phase-1 education. The length of each video was around 30- 45 min. <OPTIMIZED X-RAY MANAGEMENT> The latest activity and movement of Japan Health Physic Society “X-ray Exposure Accident Study WG” and Ministry of Health, Labor and Welfare ”Study Group on Measures to Prevent Radiation Damage from X-ray Equipment” were surveyed and discussed among the research team members.

REFERENCES:
[1] https://www.jstage.jst.go.jp/article/jhps/58/3/58_141/_article/-char/ja
[2] https://www.mhlw.go.jp/stf/newpage_37794.html

CO12-2

Development of Compensation Method for Faster Measurement with Vanadium Emitter SPND

M. Sasano, R. Tanaka[1], T. Azuma, M. Hayashi, Y. Yoshino[2] and C. H. Pyeon[2]

Advanced technology R&D center, Mitsubishi Electric corporation
[1] Energy systems center, Mitsubishi Electric corporation
[2] Institute for Integrated Radiation and Nuclear Science, Kyoto University

INTRODUCTION: For safety monitoring and control of nuclear reactors, in conventional pressurized water reactors, reactor signals are mainly measured from outside the reactor. For safer reactor control, constant monitoring inside the reactor is required in the future, and measurement inside the reactor is important for more safety opera-tion. For this purpose, the self-powered neutron detector (SPND) is one of the most suitable detectors. SPND is the detector that can obtain the signal from beta-decay associated with activation as a current, and output a current ~10 nA at 10^{12} 1/cm^2/s. SPND is suitable for measurement in high-intensity neutron environment; however, the delay in detector response due to the half-life of beta-decay is of interest in the technical issue. Previously, we examined with the rhodium (Rh) emitter SPND and succeed to compensate the time delay. In this study, we eval-uated techniques to compensate for the larger delay with the vanadium (V) emitter SPDN detector response. **EXPERIMENTS:** Measurement was conducted on 2024/10/31. We started evaluation during the 1 MW power operation. The reactor power changed from 1 MW to 5 MW during the measurement. For the measurement, we obtained current output of the V emitter SPND with an originally developed measurement unit. The period of measurement is 1 second and enough faster than the time of the reactor power increase. From these obtained data, we evaluated the compensated detector response. **RESULTS:** The results of plotting the V emitter SPND output, when the reactor was ramped up to 5 MW from 1 MW, showed that the detector output is raised with a delay of 3.74 min half-life of ^{51}V, which is the time response of the SPND (Fig. 1). The raw output current rose five time as high as that in 1 MW. From ramp up start to maxi-mum reactor power of 5 MW, it took about 20 min (5 half-life). To correct for this time response, we made the attempt to time profile deconvolution with the physical decay model. The computation of deconvolution was based on the following ^{52}V beta-decay, and the correction can be made by deriving f in Eq. (1):

$$\frac{dN}{dt} = -\lambda N + \sigma N^0 f \qquad (1)$$

where N and N^0 represent the numbers of ^{52}V and ^{51}V, respectively, σ the neutron capture cross-section of ^{51}V, and f the neutron flux from the reactor. Figure 2 shows the time variation of the raw detector output, the compensated one, and reactor power output. The increase rate in reactor power is 0.015 MW/s. The raw SPND output delayed from the increase. On the other hand, the compensated SPND output completely followed the reactor output. After reaching 5 MW, measurement result was consistent with the small deviation of the reactor power. In the previous study of the Rh emitter SPND, the compensated output slightly delayed from the increase of the reactor power. However, the compensated output completely followed the reactor output in V emitter SPND. This is because that the beta-decay scheme of V is simpler than that of Rh. For simple beta-decay scheme, the uncertainty of the time profile deconvolution is small and correctly calculated.

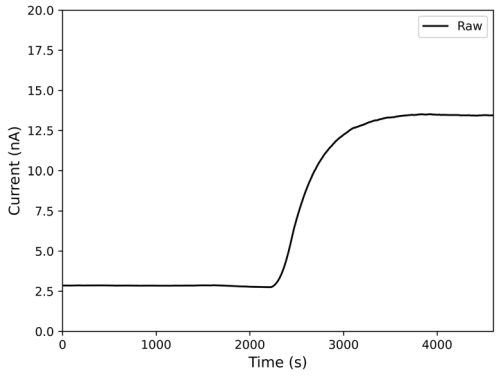

Fig. 1 The plot of normalized V emitter SPND measured current via time.

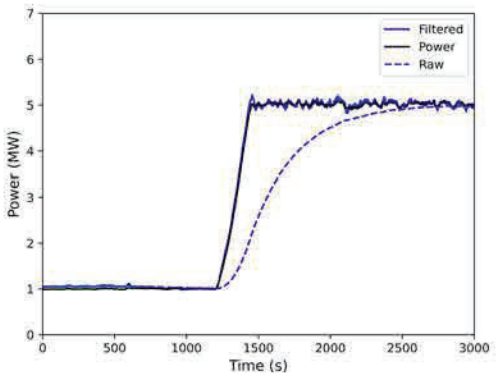

Fig. 2 The plot of V emitter SPND output and reactor power via time.

CO12-3

Measurement of U in commercially available standard solution by EDTA titration method

T. Miura[1], K. Takamiya[2], S. Fukutani[2], H. Yoshinaga[2] and Y. Iinuma[2]

[1]*National Metrology Institute of Japan, Advanced Industrial Science and Technology*
[2]*Institute for Integrated Radiation and Nuclear Science, Kyoto University*

INTRODUCTION: National Metrology Institute of Japan (NMIJ) is responsible for the development of certified reference materials and the establishment of traceability of SI (The International System of Units) to chemical metrology in Japan. To establish SI traceability, the primary method of measurements should be used to characterize the certified reference material[1)]. Uranyl ion is difficult to titrate with EDTA (ethylenediamine-N, N, N', N'-tetraacetic acid) due to its small complexation constant with EDTA. On the other hand, the logarithm of the stability constant between U(IV) and EDTA (Log $K_{U(IV)Y}$) is about 25, which allows titration at low pH (pH 1 to 3) where there is little interference from co-existing metal ions. Approximately 2 mg of U was accurately determined by EDTA titration method with repeatability of less than 0.2 % in the previous study at KURNS[3)]. In this study, the EDTA chelatometric titration method was used to measure U in a commercially available multi-element standard solution.

REAGENT and INSTRUMENTS: Dojindo Laboratories EDTA and Xylenol orange (XO) were purchased from FUJIFILM Wako pure chemicals Corporation. NMIJ CRM Bi standard solution was used for back titration. Other chemical reagents (nitric acid, acetic acid, ammonium acetate, ascorbic acid, etc.,) were analytical grade or JIS special grade. AT-510 automatic titrator (Kyoto Electronics Manufacturing Co. Ltd) was used for titration of U. HORIBA LAQUA F-72 pH meter was used for pH measurement. SPEX XSTC-4507-100 (Lot. No. 7-159-EL) muti-elemental standard solution (Ba, Be, Ca, Cs, K, U, Mg, Na, Rb, Sr, and U; 10 μg/mL) was used for sample solution.

TITRATION METOD: 50 g of sample solution in 50 mL beaker was evaporated to dryness using hot plate. After cooling, the residue was dissolved by 5 mL of 1 % HNO_3. The pH of sample solution adjusted from 3 to 4 by ammonia acetate solution. Excess amounts of 0.002 mol/kg EDTA solution and 100 mg of ascorbic acid were added to the sample solution. The sample solution was then heated and boiled on a hot plate for approximately 10 minutes to form the U(IV)-EDTA complex. After the sample solution was cooled to room temperature, acetic acid was added to the sample solution to adjust the pH from 2 to 3. Finally, 0.005 % XO solution was added to the sample solution and back titrated with 0.002 mol/kg Bi standard solution

RESULTS: U in the SPEX XSTC-457-100 was measured by EDTA titration method. The relative standard deviation of analytical results of U showed sufficient repeatability (0.63 % at sample number of 8). However, a positive bias of about 30 μg was observed in the measured values of U in each sample solution. The cause of this positive bias requires to be elucidated before applying the method to real sample.

REFERENCES:

[1] J. Vogl *et al.,* Metrologia, **55** (2018)211-221.
[2] T. Miura and A. Wada, Front. Chem., **10** (2022) 88863.
[3] T. Miura and K. Takamiya, KURNS progress report 2020 (2021) CO12-4.

CO12-4

A New Technique of the Micro bunch Interval Measurement in an Electron Linear Accelerator (II

T. Takahashi

Institute for Integrated Radiation and Nuclear Science, Kyoto University

INTRODUCTION: The coherent radiation from short bunches of electrons in an accelerator is useful of analysis of the specification of bunches. For example, it has been used in the high-resolution diagnosis of electron distribution in a bunch [1]. There are two kinds of detector in the millimeter wave region. One is a diode detector with narrow band and high-speed response. The other is a liquid-helium cooled bolometer with wide band and slow response. A bolometer is usually used with a spectrometer, for example a monochromator or an interferometer. In the experiment of FY2024 the frequency-domain measurement with a liquid-helium cooled silicon bolometer was used for the analysis of the micro bunch interval.

EXPERIMENTS: The experiment was performed with KURNS-LINAC. The energy of the electron beam was 39 MeV and the peak beam current measured by CT was 1.9 A. The repetition rate of the macro pulse was 60 pulses/s. Coherent transition radiation (CTR) from a titanium window was guided to the Fourier transform interferometer in the experimental room through the coherent radiation beam line [2]. This interferometer has maximum optical path difference (OPD) of 480 mm. The CTR was detected by the silicon bolometer.

RESULTS: The observed autocorrelation interferogram of CTR emitted from a micro bunch is shown in Fig. 1. The OPD where the intensity is minimum is 0 mm. The observed cross-correlation interferogram of CTR emitted from bunches next to each other is shown in Fig. 2. The OPD where the intensity is minimum is 230.48 mm. The theoretical interval between bunches is 230.47mm because the frequency of microwave of this linac is 1300.79 MHz. Therefore, using this method, measurements of the interval can be taken with an accuracy of 10 microns.

REFERENCES:

[1] Y. Shibata *et al.,* Phys. Rev. E, **50** (1994) 1479-1484.
[2] T. Takahashi *et al.,* Rev. Sci. Instrum., **69** (1998) 3770.

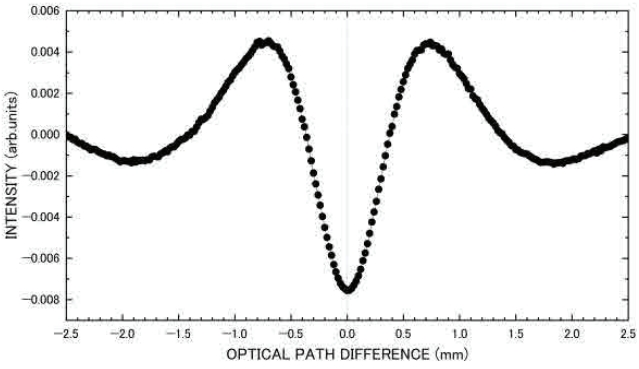

Fig. 1. observed autocorrelation interferogram of CTR emitted from a micro bunch.

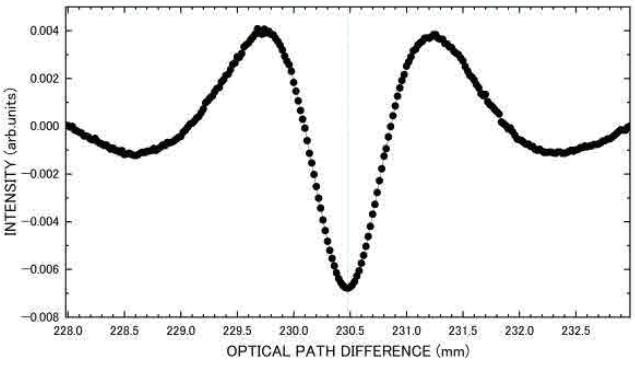

Fig. 2. The observed cross-correlation interferogram of CTR emitted from bunches next to each other.

CO12-5

A texture analysis of the excavated *Haji*-ware of different colour by INAA

M. Tomii, K. Takamiya[1], M. Inagaki[1], Y. Chiba[2], A. Ito[2], M. Kidachi[3], and H. Yoshii[2]

Faculty of Literature, Taisho University
[1] *Institute for Integrated Radiation and Nuclear Science, Kyoto University*
[2] *Graduate School of Letters, Kyoto University*
[3] *College of Letters, Ritsumeikan University*

INTRODUCTION: To investigate the reason for the difference of the medieval low-temperature-fired pottery (Haji-ware) in colour –white/red–, a collection of Haji-ware of 14th century archaeo-logically excavated in the campus of Kyoto University [1] is analysed. The two major types, white larger bowl and reddish medium-sized plate, are done from the single deposition unit. As for the colour difference, some scholars assume that white ones resulted from the water-sieving of clay to decrease iron oxide while others point out that they could result from the reducing condition of firing. Last year, we analysed the different collection of the Haji-ware of the same age and suggested that the colour difference might be due to the difference in clay texture in the light of Na/La concentrations combination, but we did not check the ratio of long-lived nuclides including Fe. This year we there-fore try to check both short-lived and long-lived ones in detail.

EXPERIMENTS: Conventional INAA was applied to determine the elemental composition of samples of the Haji-ware, each of whose main body had been drilled, or scraped, by the alumina drill into fine powder as a sample after removing off the very surface and then had been enclosed in a polyethylene bag [2]. Every of above-mentioned two types of the Haji-ware has seven samples re-spectively from different pieces. Each of the fourteen samples was neutron-irradiated at Pn-3 (1 MW for 90 seconds) for short-lived nuclides, and at Pn-2 (5 MW for 1 hour) for long-lived ones. The gamma-ray spectrometry of the irradiated samples was performed after the irradiation, and the k0-standardization method for determination of concentration of elements was performed. For the k0 method, three standard elements, Au, Lu and Zr, were prepared as a comparator.

RESULTS: Concentrations of twenty elements in almost every fourteen sample were determined with irradiation by Pn-3 and Pn-2: Co, Cr, Cs, Eu, Fe, Ga, Hf, K, La, Mg, Mn, Na, Rb, Sc, Sm, Ta, Tb, Th, Ti, and V. While Na/La concen-trations combination does not necessarily coincide with the colour difference, Fe shows the marked difference along with the colour difference (Figs.1 and 2). These results indicate that the La-rich clay group might usually undergo the process of decreasing Fe_2O_3 to produce white-coloured ware while a little portion in the group occasionally escape the process such as KC11-1199, 1227, and 1228, leading to the reddish ware.

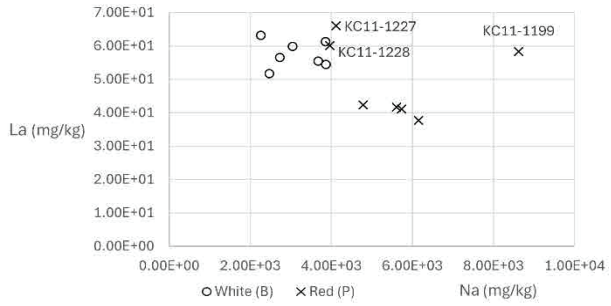

Fig. 1 Distribution of fourteen samples on the concentrations combination of Na with La.

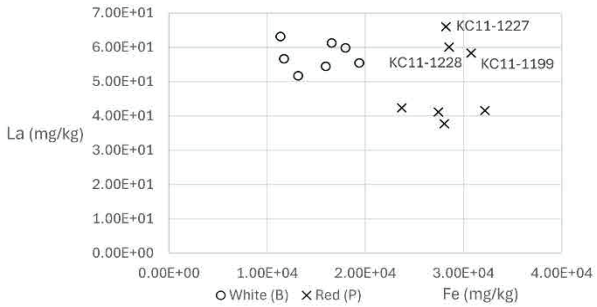

Fig. 2 Distribution of fourteen samples on the concentrations combination of Na with Fe.

REFERENCES:

[1] M. Tomii *et al., Annu. Rept. of Archaeological Researches in KU sites for 2013*. (2015) 5-122.
[2] J. Sterba, *J. Radio. Nucl. Chem.,* **316** (2018) 753-759.

CO12-6

Elucidation of the structural dynamics of E6AP ubiquitin ligase

H. Konno[1], M. Shimizu[2], K. Morishima[2], R. Inoue[2], M. Sugiyama[2]

Graduate School of Science, Kyoto University
[1]Nano Life Science institute, Kanazawa University
[2]Institute for Integrated Radiation and Nuclear Science, Kyoto University

INTRODUCTION: It is known that E6AP (E6-associated protein), a kind of ubiquitin ligase, interacts with E6 protein derived from oncogenic human papilloma virus (HPV 16/18) and the enzyme complex induces ubiquitination of p53 resulting p53 degradation by ubiquitin-proteasome system. To understand the mechanism of p53 ubiquitination by E6AP and E6, we use HS-AFM to observe the structural dynamics of the E6AP/E6 complex. In addition to HS-AFM observation, we analyze the structural dynamics of the E6AP/E6/p53 complex using small-angle X-ray scattering (SAXS) methods.
****

EXPERIMENTS : HS-AFM observation of E6AP, E6AP/E6 and E6AP/E6/p53. HS-AFM imaging of the full-length E6AP, E6AP/E6 complex and E6AP/E6/p53 complex in solution were performed using a laboratory-built HS-AFM setup [1, 2]. SAXS and ultracentrifugation analysis of E6AP. The SAXS was performed using NANOPIX (Rigaku). Changing sample solution, the scattering profiles were measured four times with sample-detector distance of 1330 mm, and data from the first 15 minutes of each measurement were used for analysis. Similarly, the scattering profiles were also measured five times with sample-detector distance of 300 mm, and data from the first 60 minutes of each measurement were used for analysis.
****

RESULTS :HS-AFM observation of E6AP, E6AP/E6 and E6AP/E6/p53. By using of HS-AFM, We found that the importance of the N-terminal region with respect to the p53 binding to E6AP/E6. SAXS and ultracentrifugation analysis of E6AP. The scattering intensity appears to be concentrated in the larger scattering vector (Q) region (Fig. 1). This is due to the effect of aggregation of the HECT domain due to multimerization, and we found that the results may be slightly different from the original structural information. We also performed analytical ultracentrifugation (Fig. 2), and the sample contained not only E6AP alone, but also a degradation product from the protein purification process and a multimerized protein.
****

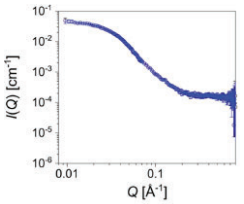

Fig. 1. X-ray scattering profile of full length E6AP.

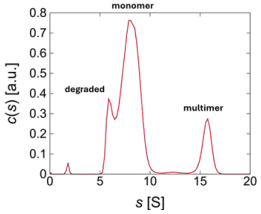

Fig. 2. Analytical ultracentrifugation of full length E6AP

REFERENCES:
[1] T. Uchihashi *et al.,* Nat. Protoc., **7** (2012) 1193-1206.
[2] T. Ando *et al.,* Chem. Rev., **114** (2014) 3120-3188.

CO12-7

Development of an Analog Encoder Module

H. Ohshita[1], H. Endo[1], T. Seya[1], S. Matoba[1] and M. Hino[2]

[1]*Institute of Materials Structure Science, KEK*
[2]*Institute for Integrated Radiation and Nuclear Science, Kyoto University*

INTRODUCTION: The analog encoder (AE) was developed as a readout module for use in pulsed neutron experiments. The AE can measure the TOF and pulse height of the input analog signal. The pulse height can be used to derive the detection position in addition to conducting nγ discrimination. Figure 1 shows the AE, which has four analog inputs and a T0 input for resetting the TOF. The dynamic range of the analog input is 0 to -2 V, and the T0 input is designed for transistor-transistor logic (TTL)- or Nuclear Instrumentation Module (NIM)-level inputs. The signal level of the T0 input can be changed by the internal jumper switch. Both analog and T0 inputs are terminated at 50 Ω. In addition, there are four digital inputs (switchable between TTL and NIM levels). The AE operates at an internal clock speed of 200 MHz, giving it a time accuracy of 5 ns. The data encoded in the AE are transferred to a computer over a 1-Gbps network. Transmission Control Protocol (TCP) communication is used for data transfer between the AE and a computer, whereas User Datagram Protocol (UDP) communication is used for control, such as parameter setting. The analog and digital inputs implemented in the AE operate independently. Therefore, it is necessary to cluster multiple channels in an offline analysis to derive the detection position. When the detection position is derived based on the ratio of the pulse height values of the analog signals output from the four corners of the readout board, the shapes of these signals should be similar, and the data generated by the AE contain parameters for finding such signals. Data encoded from the analog inputs include information on the TOF, maximum pulse height, pulse width, and rise time. Data encoded from digital inputs provide information on TOF and pulse width. Clustering between different channels is performed by setting a time window in offline analysis and collecting events with similar TOFs.

EXPERIMENTS: A neutron irradiation test using a prototype AE was conducted in February 2025 at the KUR CN-3. A scintillation detector was installed downstream of the CN-3 disk chopper. The detector consisted of 0.8-mm-thick enriched lithium glass (Scintacor Ltd., GS-20) and a multi-anode photomultiplier tube (HAMAMATSU PHOTONICS K. K., H12700A-03). The active area of the scintillation detector was 48.5×48.5 mm, and analog signals were output from the four corners of the readout board (HAMAMATSU PHOTONICS K. K., E14340) using a resistance chain. A collimator made of boron carbide was installed in front of the scintillation detector. The aperture of the collimator was 1×1 cm. In the neutron irradiation test, the flight time was measured according to the timing of the disk chopper opening. Figure 2 shows the TOF distribution and two-dimensional hit map obtained from the test. The peak of the TOF distribution corresponds to thermal neutrons of 2 Å. In addition, the two-dimensional hit map represents the beam profile blocked by the collimator. The detection positions were calculated in offline analysis. Future plans include evaluating the validity of the measurement data and improving the AE.

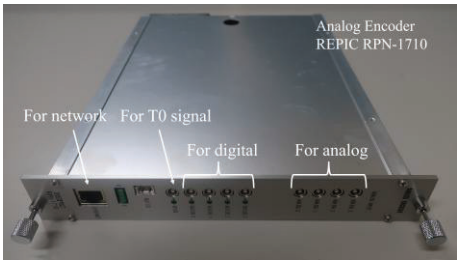

Fig. 1. Picture of the AE.

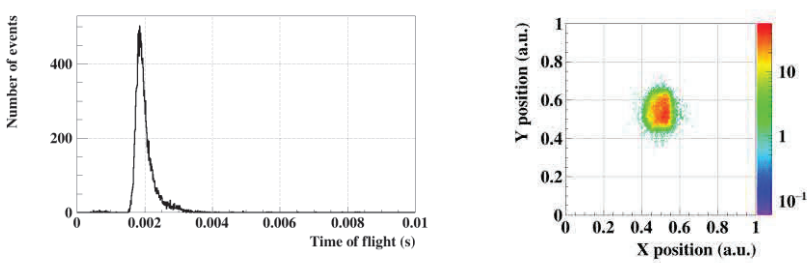

Fig. 2. Test results: TOF distribution (left) and 2D-hit map (right).

CO12-8

Application of KURAMA-II to the analysis of air dose rate distribution around monitoring posts

M. Hosoda[1], M Watanabe[1], H Tanaka[1], M. Tanigaki[2]

[1]*Japan Chemical Analysis Center*
[2]*Institute for Integrated Radiation and Nuclear Science, Kyoto University*

INTRODUCTION: In the nationwide survey of environmental radioactivity levels commissioned by the Nuclear Regulation Authority, air dose rates are measured using portable monitoring posts at about 80 locations in Fukushima Prefecture. Air dose rates obtained by monitoring posts are representative values for each location, and we do not see the detailed distribution of the air dose rate due to the uneven distribution of the artificial radionuclides around the monitoring posts.

In this study, we measured air dose rates around the portable monitoring posts located in a difficult-to-return zone in Fukushima Prefecture by a car-borne survey system KURAMA (Kyoto University Radiation MApping system)- Ⅱ as a walking survey. We analyzed the distribution of the air dose rate and the radioactive cesium using radiation mapping methods.

EXPERIMENTS: We walked with KURAMA-II around the monitoring post at the Kumamachi Elementary School in Okuma Town, Fukushima Prefecture. The data were grouped by a 1 m mesh centered on the monitoring post, and an areal evaluation was performed by displaying the data on a map. From the measured air dose rate data and the pulse-height spectrum data of each mesh, the air dose rate from the natural radioisotopes and that given by the artificial radioisotopes, i.e., Cs-134 and Cs-137, were evaluated respectively using Equation (1) defined in ref. [1],

$$\begin{cases} \dot{D}_n = 0.062x \\ \dot{D}_a = \dot{D}_t - \dot{D}_n \end{cases} \quad (1)$$

where - $\dot{D}_t$ is the measured air dose rate (μSv/h), x is the counting rates from 1400 to 2000 keV obtained by spectrum data, $\dot{D}_n$ is the air dose rate given by natural radioisotopes, and $\dot{D}_a$ is that given by the artificial radioisotopes.

RESULTS: Figure 1 shows the 1 m × 1 m mesh map of the air dose rate obtained by the present walking survey. The average air dose rate measured by the monitoring post was 2.09 μGy/h, whereas the average air dose rates per 1 m × 1 m mesh obtained by the walking survey ranged from 1.32 to 4.11 μGy/h. The overall average value for all meshes was 2.10 μGy/h, which was similar to the average value from the monitoring posts. Figure 2 shows the map display of the air dose rate given by natural radioisotopes for each mesh calculated by Equation (1). From Figure 1 and 2, the differences in the air dose rates are not due to the uneven distribution of natural radioisotopes but the artificial radioisotopes.

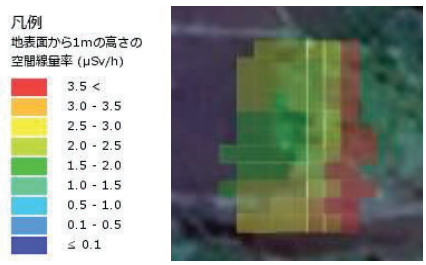

Figure 1. the 1 m × 1 m mesh map of the air dose rate(μSv/h) obtained by the present walking survey.

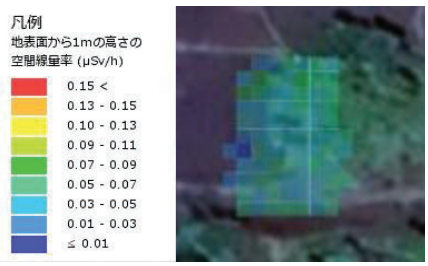

Figure 2. The map display of the air dose rate (μSv/h) given by natural radioisotopes for each mesh calculated by Equation (1).

REFERENCES:

[1] M Ando, N Matsuda and K Saito, "Determination of Parameters for an Equation to Obtain Natural Background Radiation Using KURAMA-II Loaded with C12137-01 CsI(Tl) Detector," *T. J. At. Energy Soc. Jpn.*, **20**[1], 34-39 (2021)

CO12-9

Relationship between Friction Reduction Effect and Solubility in Base Oil of Organic Friction Modifiers

T. Hirayama, H. Gu, N. Yamashita[1] and M. Hino[2]

Department of Mechanical Engineering and Science, Graduate School of Engineering, Kyoto University
[1]Department of Mechanical and System Engineering, Kyoto Institute of Technology
[2]Institute for Integrated Radiation and Nuclear Science, Kyoto University

INTRODUCTION: Lubricants are essential in minimizing frictional forces and reducing surface wear in industrial machinery. This study explored the relationship between the solubility of additives in base oils and their friction-reduction efficacy using cetyl alcohol as a model additive. Atomic force microscope (AFM) friction tests demonstrated that the friction reduction effect of cetyl alcohol varied significantly across the base oils. The solvation free energy was computed using molecular dynamics (MD) simulation to evaluate the solubility of cetyl alcohol in various base oils. A direct proportional relationship between friction reduction and solvation free energy was observed, indicating that additives with lower solubility have better friction-reduction performance. Neutron reflectometry experiments and further MD simulations revealed that lower solubility correlates with stronger adsorption of additives on the substrate. This study quantitatively clarified the relationship between solubility, adsorption, and friction reduction, providing insights into optimizing lubricant formulations for enhanced performance and contributing to a deeper understanding of the mechanisms behind boundary lubrication.

EXPERIMENTS: Cetyl alcohol (>98%, Sigma) was used as a model additive due to its friction-reduction and anti-wear effects in base oils. Seven common organic solvents were used as base oils: dodecane (C12), tetradecane (C14), hexadecane (C16), isocetane (IC), squalane (Sq), dodecylbenzene (DB) and dodecyl acetate (DA). Deuterated cetyl alcohol (CDN Isotopes Inc.) was used to achieve a good contrast of the scattering length density (SLD) with base oils for the NR measurements. Its concentration was set to 0.5 mass% to achieve a more pronounced contrast.

RESULTS: The adsorption behavior of cetyl alcohol molecules on Fe surfaces in various base oils was analyzed using NR. The reflectivity profiles in the left show the experimental data as triangles and the results fitted using GenX 3 software as solid black lines. For Sq, IC, and C16, a leftward shift in the reflectivity profiles was observed upon the introduction of cetyl alcohol, compared with the profiles of the base oil alone.Correlating with the friction experiments, these three solvents exhibited the greatest friction reduction upon the addition of cetyl alcohol. In contrast, for DB and DA, no appreciable shift in the reflectivity profiles was detected, suggesting the absence of an adsorption layer. The pattern of adsorption layer density values is consistent with that of friction reduction: higher adsorption layer densities correlate with more effective friction reduction. We attribute this to the relatively weak adsorption characteristics of alcohols and the challenge of detecting adsorption films at lower concentrations. These results indicate that the lower the solubility of the additive molecules in the base oil, the larger the friction reduction. As confirmed by the NR measurements, the lower the solubility, the denser the additive adsorption film formed, which leads to a reduction in the COF.

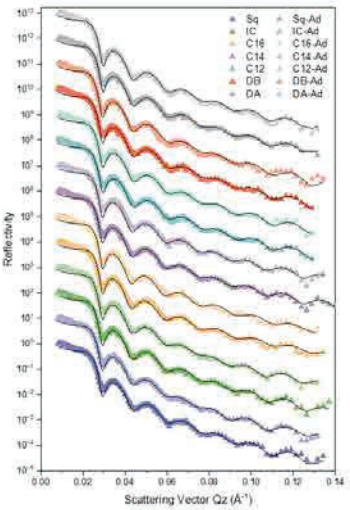

Fig. 1. Reflectivity profiles for all sets of lubricants.

CO12-10

Directional Evaluation of Internal Pores in Additively Manufactured Metal Using Neutron Phase Imaging

Y. Seki, Y. Terakawa[1]. M. Hino[2]

Institute of Multidisciplinary Research for Advanced Materials, Tohoku University
[1]Graduate School of Engineering, Tohoku University
[2]Institute for Integrated Radiation and Nuclear Science, Kyoto University

INTRODUCTION: Neutron scattering (dark-field) imaging [1, 2] using a Talbot-Lau interferometer can detect small-angle scattering intensity caused by microscopic structures within a sample. When employing an interferometer composed of one-dimensional gratings, the method is sensitive to scattering perpendicular to the grating lines. By rotating the sample with respect to the grating orientation, scattering in different directions can be observed, allowing for the assessment of anisotropy in the microstructure. In this study, we applied this method to an additively manufactured metal sample and investigated the characteristics of internal pores.

EXPERIMENTS: The sample was a 1 cc stainless steel cube fabricated using the laser powder bed fusion method, with laser power and scan speed intentionally set lower than standard process parameters. The sample was first imaged with its stacking direction (z-direction) aligned parallel to the grating lines of the interferometer, as shown in Fig. 1(a) and (b). In this configuration, scattering in the y-direction was detected. The sample was then rotated 90 degrees around the beam axis, and an additional image was acquired to observe scattering in the z-direction, as shown in Fig. 1(c).

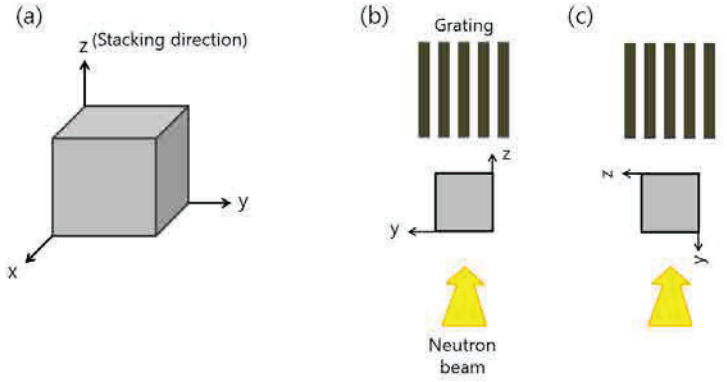

Fig. 1. (a) Coordinate system of the sample. (b) Measurement configuration for scattering in the y-direction. (c) Measurement configuration for scattering in the z-direction.

RESULTS: Figure 2(a) and (b) show the scattering images obtained in the configurations illustrated in Fig. 1(b) and 1(c), respectively. In these scattering images, darker regions correspond to stronger scattering. In Fig. 2(a) and Fig. 2(b), the average visibility reduction within the sample region was 0.40 and 0.30, respectively. These results suggest that the size of pores in the sample tend to be longer in the y-direction and shorter in the z-direction.

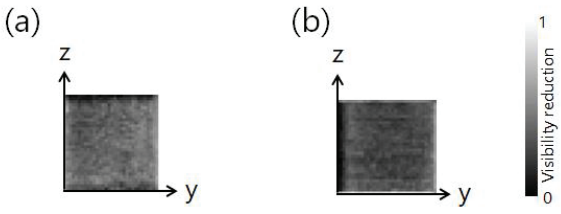

Fig. 2. Scattering images from (a) y-directional and (b) z-directional configurations.

REFERENCES:

[1] W. Yashiro *et al.*, Opt. Exp 18, 16890 (2010). [2] M.Strobl *et al.*, Sci. Rep. 4, 7243 (2014).

CO12-11

Evaluation of the Autocorrelation Length in Neutron Scattering Imaging at the CN-3 Port

Y. Seki, Y. Terakawa[1], T. Higuchi[2], M. Li[2], M. Hino[2]

Institute of Multidisciplinary Research for Advanced Materials, Tohoku University
[1]Graduate School of Engineering, Tohoku University
[2]Institute for Integrated Radiation and Nuclear Science, Kyoto University

INTRODUCTION: In neutron phase imaging using a grating interferometer, scattering imaging (dark-field imaging) [1, 2] can visualize the small-angle scattering intensity caused by microstructures in the sample as a reduction in the visibility of the interference pattern. This reduction is related to the autocorrelation function $\Phi(x)\Phi(x + \Delta x)$ of the phase shift of neutron waves generated in the sample. The parameter representing the spatial shift Δx in the autocorrelation function is called the autocorrelation length, which can be varied by changing the sample position within the interferometer. By performing measurements at various autocorrelation lengths, the characteristics of the microstructures can be quantitatively evaluated. In the current setup of our Talbot-Lau interferometer [3] at the CN-3 port of KUR, the sample is usually placed between the middle phase grating (G1) and the most downstream analyzer grating (G2), which are spaced 140 mm apart. However, depending on the sample size, it is more convenient to place the sample upstream of G1. Therefore, we conducted evaluations of the autocorrelation length with the sample positioned upstream of G1, using a reference sample whose reduction rate as a function of autocorrelation length has been well characterized between G1 and G2.

EXPERIMENTS: The reference sample was a 1 cc cube of aluminum alloy (Al–10%Si–0.4%Mg), additively manufactured using the laser powder bed fusion method with standard process parameters. Micropores with diameters on the order of micrometers induced small-angle neutron scattering. Measurements were performed at six positions located 10 mm, 110 mm, 210 mm, 505 mm, 605 mm, and 705 mm upstream from G1. The exposure time at each position was 640 s, with the reactor thermal power of 5 MW.

RESULTS: Figure 1 shows a plot of the observed visibility reduction rate, averaged over the sample region. The autocorrelation lengths corresponding to each sample position were calculated based on Ref. [2]. The solid line in the figure represents a model curve derived from the reduction rate measured between G1 and G2. Although the maximum autocorrelation length in the G1–G2 configuration is currently 3.4 μm, the curve is extrapolated beyond this range. The model curve and the measured values show good agreement. Furthermore, an autocorrelation length of approximately 4.0 μm was achievable just upstream of G1.

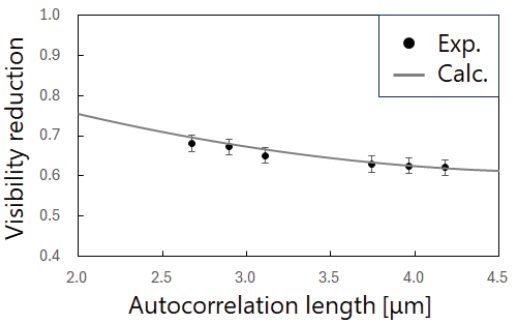

Fig. 1. Comparison of visibility reduction measured upstream of G1 and between G1 and G2.

REFERENCES:

[1] W. Yashiro *et al.*, Opt. Exp 18, 16890 (2010).
[2] M.Strobl *et al*., Sci. Rep. 4, 7243 (2014).
[3] Y. Seki *et al*., Rev. Sci. Instrum., 94, 103701 (2023).

CO12-12

Observation of Internal Pore Distribution in Additively Manufactured Metal

Y. Seki, Y. Terakawa[1]. T. Higuchi[2], M. Li[2], M. Hino[2]

Institute of Multidisciplinary Research for Advanced Materials, Tohoku University
[1]Graduate School of Engineering, Tohoku University
[2]Institute for Integrated Radiation and Nuclear Science, Kyoto University

INTRODUCTION: Metal additive manufacturing is a highly promising technique owing to its ability to produce complex geometries with reduced weight and advanced functionality. However, due to the layer-by-layer melting and solidification process, it tends to generate microscopic pores within the material during the fabrication. The porosity of the fabricated material is typically inves-tigated through destructive testing, such as cross-sectional observation using optical microscopy. Currently, it is difficult to non-destructively assess the porosity distribution throughout the overall structure. We are developing a non-destructive technique using neutron phase imaging [1] at the CN-3 port of KUR to visualize the porosity distribution inside additively manufactured metal structures. By observing the small-angle neutron scattering effects caused by micropores using a grating interferometer, we can gain insights into the interior of relatively thick structures. This ap-proach also allows us to observe a wide area over several tens of square centimeters. In this study, we attempted to estimate the distribution of internal pores using a simple method based on imaging from three different directions.

EXPERIMENTS: The observed sample was a 1 cc stainless steel cube fabricated using the laser powder bed fusion method. Since it was produced with a laser power intentionally set above standard process parameters, numerous micropores were expected to be formed within the structure. As shown in Fig. 1(a), the sample was irradiated with neutron beams along the x-, y-, and z-axes, and scattering images were obtained for each direction.

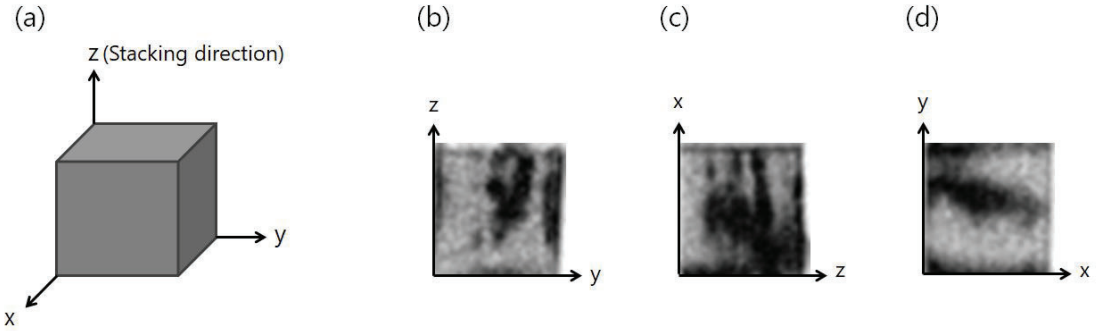

Fig. 1. (a) Coordinate system of the sample. (b) Scattering image observed from x-direction. (c) From y-direction. (d) From z-direction.

RESULTS: Figure 1(b), (c), and (d) shows resultant images observed from three directions. The darker regions in the images correspond to areas with a higher concentration of pores. A simple back-projection of these three images was used to estimate the internal pore distribution, as shown in Figure 2. The figure illustrates an example of the pore distribution on an oblique cross-sectional plane.

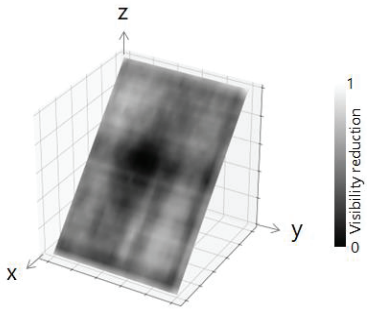

Fig. 2. Estimated internal pore distribution based on three scattering images.

REFERENCES:

[1] Y. Seki *et al*., Rev. Sci. Instrum., 94, 103701 (2023).

CO12-13

Study of Isotope Separation via Chemical Exchange Reaction

R. Hazama, P. Kumsut, T. Yoshimoto, A. Rittirong[1], C. Pitakchaianan, K. Kosinarkaranun, Y. Sakuma[2], T. Fujii[3], T. Fukutani[4], Y. Shibahara[4], and T. Kishimoto[1]

Graduate School of Human Environment, Osaka Sangyo University
[1]Research Center for Nuclear Physics, Osaka University
[2]Laboratory for Zero-Carbon Energy, Institute of Science Tokyo
[3]Graduate School of Engineering, Osaka University
[4]Institute for Integrated Radiation and Nuclear Science, Kyoto University

INTRODUCTION: Chemical isotope separation for calcium and lithium has been studied by liquid-liquid extraction (LLE) with DC18C6 crown-ether [1]. This report describes LLE with 5ml of 30%(w/w) LiCl and 100ml of 0.07M B15C5 dissolved in chloroform.

EXPERIMENTS: Chemical Isotopic exchange occurs according to the following chemical exchange reaction: $^{6}Li^{+}_{(aq)} + {}^{7}LiL^{+}_{(org)} \rightarrow {}^{6}Li^{+}_{(aq)} + {}^{7}LiL^{+}_{(org)}$ (1)
, where L represents macrocyclic polyether (B15-crown-5). Lithium chloride solution (30% LiCl (aq) was mixed in an Erlenmeyer flask with 0.07M B15C5 dissolved in chloroform by the volume ratio of 1/20 (aqueous/organic) by a magnetic stirrer, The extraction time was kept consistent at 1 min and the phase separation time in the separation funnel was 10 min. To retrieve the lithium in the organic phase, 10 ml pure water was mixed with the extraction time and phase separation time of 10 min.

RESULTS: As shown in Fig. 1, the separation factor (α) was obtained by multi-stage LLE (eight iteration) with and without 12 M hydrochloric acid (HCl) at room temperature (22±0.5℃). It is noted that our recent progress in the measurement of isotope ratio for calcium and lithium was carried out by utilizing the cool plasma technique and the result obtained by TIMS was generally consistent [4].

Ref.	Chemical species	Distribution Coefficient (D)	Single stage separation factor	Temperature (℃)	Initial concentration of B15C5
[2]	LiCl	6.0×10^{-2}	1.002±0.002	22±0.5	0.07 M
[3]	LiCl	1.62×10^{-5}	1.002±0.002	25	0.186 M
[3]	LiI	1.58×10^{-3}	1.026±0.002	25	0.186 M
[3]	LiSCN	5.40×10^{-3}	1.032±0.002	25	0.186 M

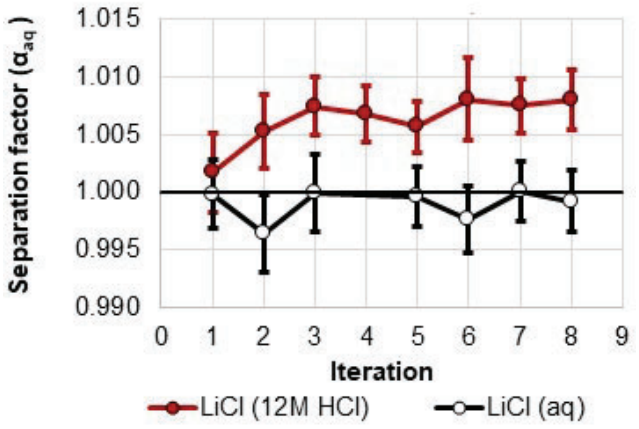

Fig. 1. Separation factor (α) of litium isotope in the aqueous phase with (filled) and without 12M HCl (open). [2].
($\alpha=([^{6}Li]/[^{7}Li])_{org}/([^{6}Li]/[^{7}Li])_{aq}$).

REFERENCES:

[1] A. Rittirong, Doctor Thesis, OSU (2022).
[2]P. Kumsut, to be published in J. Phys:Conf Series (SPLG2023).
[3]K. Nishizawa et al, J. Nucl. Sci. Tec.21,694(1984): K. Nishizawa et al, J. Nucl. Sci. Tec.21,133(1984).
[4]A. Ishikawa and M.Nomura, in private communication.

CO12-14

Developing a new method for determining ionization chamber response ratio between air and P-10 gas for ^{41}Ar calibration applications

R. Furukawa[1], H. Yashima[2], Y. Soeta[3], R. Ichikawa[3], S. Otsuka[3], H. Murata[3], R. Nagata[4] and T. Yamada[3,5]

[1]*National Metrology Institute of Japan, Advanced Industrial Science and Technology*
[2]*Institute for Integrated Radiation and Nuclear Science, Kyoto University*
[3]*Graduate School of Science and Engineering Research, Kindai University*
[4]*Fuculty of Science and Engineering, Kindai University*
[5]*Atomic Energy Research Institute, Kindai University*

INTRODUCTION: In order to calibrate gas monitors used in nuclear facilities for measuring radioactive noble gases, use of activity reference measurement standard gases with known activity are essential. Among these gases ^{41}Ar is a representative nuclide released from nuclear reactors. While a primary activity standard for ^{41}Ar is currently under development at the National Metrology Institute of Japan (NMIJ) [1], activity standard for ^{85}Kr have already been established based on measurement using a set of proportional counters of different length [2]. Commercially available gas monitors are typically designed to measure radioactive gas concentration in air, not in P-10 counting gas. Therefore, calibration should ideally be performed using air as the detection medium. However, proportional counters generally do not work well when air is used as the counting gas. In response to this limitation, we designed a calibration system using an inner-through type ionization chamber capable of operating both P-10 gas and air. This system serves as a transfer standard for calibrating gas monitors. To determine ^{41}Ar concentration using the ionization chamber, it is necessary to evaluate in advance its response, specifically, the conversion factor from ionization current into to ^{41}Ar activity concentration. Although preliminary studies have assessed the chamber's response to ^{41}Ar in P-10 gas [1], the response ratio between air and P-10 gas has not yet been established. This study proposes a method to derive that response ratio using a gas substitution and extrapolation technique.

****

EXPERIMENTS: Two 3 ml acrylic containers were filled with pure argon gas. ^{41}Ar gas was produced via ^{40}Ar(n, γ)^{41}Ar reaction by irradiating the gas samples for 60 s at the at the bottom of KUR-SLY reactor operating at 1 MW thermal output. The production of ^{41}Ar was confirmed gamma-ray spectroscopy using a HPGe detector. In the proposed “extrapolation method”, a mixture of ^{41}Ar and P-10 was initially prepared. Half of gases was then evacuated and replaced with dry air. This step was repeated twice, resulting in gas mixtures with P-10 to air ratios of 100 : 0, 50 : 50, and 25 : 75. The ionization current was measured at each stage. To account for dilution effect, measured currents were corrected based on the proportion of P-10 in the mixture and normalized to the current measured at 100% P-10. Assuming the ^{41}Ar activity remained constant throughout, a regression line was fitted to the normalized data using the least-squares method. The intercept of this regression line represents the ionization current corresponding to 100 % air, relative to that for 100 % P-10, thereby yielding the response ratio.

****

RESULTS: The response ratio of the ionization chamber when filled with air compared to P-10 gas was determined to be 0.680. In future work, the reliability of this extrapolation method will be assessed by conducting uncertainty evaluation and comparing it with alternative measurement approaches.

****

REFERENCES:

[1] A. Yunoki *et al.*, KURNS Progress Report 2019, (2020) CO12-5, 275.
[2] A. Yunoki *et al.,* Appl Radiat Isot., **68(7-8)** (2010) 1340-1343.

CO12-15

Effect of the Charging State of a Lithium-Ion Battery on the Positron Annihilation Characteristics in Graphite Anode

A. Yabuuchi, N. Oshima[1], T. Fujiwara[1], K. Michishio[1], and M. Hino

Institute for Integrated Radiation and Nuclear Science, Kyoto University
[1]National Institute of Advanced Industrial Science and Technology

INTRODUCTION: Positron annihilation spectroscopy typically requires positrons to be injected from the sample surface, limiting its ability to probe the interior of thick samples. In this study, a lithium-ion battery (LIB) was irradiated with thermal neutrons to produce the positron-emitting nuclide ^{64}Cu in the copper foil anode current collector, enabling the investigation of positron annihilation characteristics in the graphite anode. We previously observed changes in positron annihilation characteristics during Li-ion deintercalation (i.e., discharge). To determine whether the observed changes were significant, we evaluated the temporal stability of the *S* parameter under no-charge/discharge conditions in this fiscal year.

EXPERIMENTS: The LIB sample was irradiated with thermal neutrons at the KUR CN-3 port for 24 h at 1 MW and 6 h at 5 MW. Following irradiation, and in accordance with previous experimental protocols, the sample was left for about 24 h before measuring the annihilation gamma-rays emitted from positrons injected into the graphite anode using a high-purity Ge detector. The temporal changes in the Doppler broadening of the annihilation radiation spectrum were characterized using the *S* parameter [1]. A series of measurements was conducted under two conditions: the same LIB sample in a discharged state and a half-charged state.

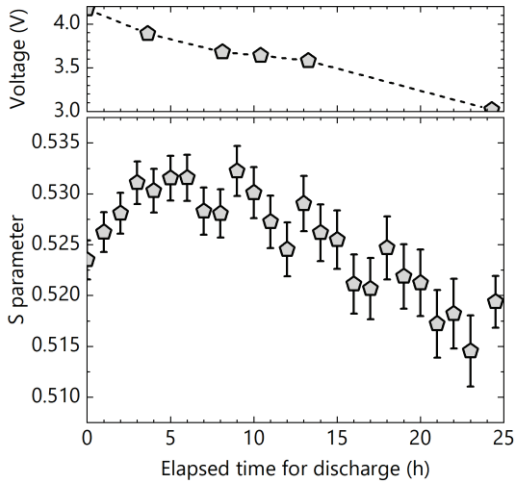

Fig. 1. *S* parameter changes while discharging. The upper panel shows the closed-circuit voltage.

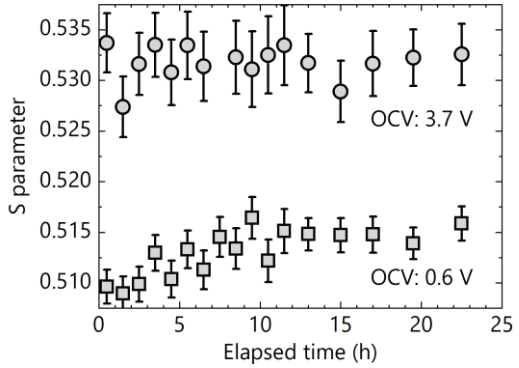

Fig. 2. Time variation of the *S* parameters in different charge states. The open-circuit voltage (OCV) of 0.6 V and 3.7 V correspond to the discharged and half-charged states, respectively.

RESULTS: Figure 1 shows the changes in the *S* parameter during the discharging of a graphite anode from a fully charged state. During discharge, the *S* parameter initially increases and then decreases, consistent with our first-principles calculations. Figure 2 shows the temporal evolution of the *S* parameter measured at open-circuit voltages (OCVs) of 0.6 V (fully discharged state) or 3.7 V (half-charged state), under conditions without charging/discharging during measurements. (Note that an OCV of 0.6 V corresponds to an over-discharged state.) These results indicate that the *S* parameter strongly depends on the LIB's charge state. However, at an OCV of 0.6 V, a gradual increase in the *S* parameter is observed during the first 10 hours, possibly influenced by the 847 keV gamma-ray peak of ^{56}Mn, which has a higher energy than the 511 keV annihilation photopeak. (Mn is present in the cathode material.) Since the half-life of ^{56}Mn (2.6 h) is shorter than that of ^{64}Cu (12.7 h), its influence diminishes over time.

REFERENCES: [1] F. A. Selim, Mater. Charact. **174** (2021) 110952.